



# Introducing graphene (reduced graphene oxide) into Al matrix composites for enhanced high-temperature strength

Y.N. Zan<sup>a,c,1</sup>, Q. Zhang<sup>a,c,1</sup>, Y.T. Zhou<sup>a</sup>, Z.Y. Liu<sup>a</sup>, Q.Z. Wang<sup>b</sup>, D. Wang<sup>a</sup>, B.L. Xiao<sup>a,\*\*</sup>, W. C. Ren<sup>a</sup>, Z.Y. Ma<sup>a,\*</sup>

<sup>a</sup> Shenyang National Laboratory for Materials Science, Institute of Metal Research, Chinese Academy of Sciences, 72 Wenhua Road, Shenyang, 110016, China

<sup>b</sup> Key Laboratory of Nuclear Materials and Safety Assessment, Institute of Metal Research, Chinese Academy of Sciences, 72 Wenhua Road, Shenyang, 110016, China

<sup>c</sup> School of Materials Science and Engineering, University of Science and Technology of China, 72 Wenhua Road, Shenyang, 110016, China

## ARTICLE INFO

### Keywords:

Aluminium matrix composites  
Graphene  
High-temperature strength  
Mechanical properties  
Thermal stability

## ABSTRACT

Lamellar amorphous Al<sub>2</sub>O<sub>3</sub> (am-Al<sub>2</sub>O<sub>3</sub>) in Al<sub>2</sub>O<sub>3</sub>/Al composites exhibits extreme strengthening effect on high-temperature strength, but suffers from efficacy loss because of crystallizing into granular γ-Al<sub>2</sub>O<sub>3</sub> at temperatures over 450 °C. Here, based on the existing solution-mixing process, reduced graphene oxide (rGO) sheets were introduced into Al<sub>2</sub>O<sub>3</sub>/Al composite to enhance its high-temperature strength for the first time. It was shown that rGO sheets within the am-Al<sub>2</sub>O<sub>3</sub> films could prevent them from transforming into γ-Al<sub>2</sub>O<sub>3</sub> in the high-temperature hot-pressing processes. As a result, by addition of a very small number of rGO sheets, the composites were strengthened significantly at both room and high temperatures. Strengthening mechanisms at room and high temperatures were discussed. Furthermore, enhanced thermal stability of am-Al<sub>2</sub>O<sub>3</sub> was explained by thermodynamics and kinetics factors. This work provides a novel application of graphene in structural materials.

## 1. Introduction

Al alloys and composites with stable microstructure and mechanical properties at elevated temperatures are highly desired in military defense, transportation, nuclear industry and other fields, especially for applications at over 300 °C [1–3]. Although age-hardened aluminium alloys exhibit high strength at room temperature (RT), their strength values at elevated temperatures are quite insufficient [1,2,4]. Usual precipitates such as Mg<sub>2</sub>Si, CuAl<sub>2</sub>, MgZn<sub>2</sub> etc. would be coarsened/dissolved and lose strengthening efficiency rapidly at ~200 °C because of diffusion of the alloying elements [3–5], therefore, thermally stable Al materials are in high demand.

Al-Fe series heat-resistant Al alloys fabricated by rapid solidification process exhibited high high-temperature strength, due to the strengthening by metastable dispersoids [6–8]. However, its poor ductility presented a challenge to the application, and more seriously, the metastable dispersoids, according to different investigations [7,9–11], would also coarsen at 400–500 °C or transform into coarse equilibrium phase, which brings great difficulty to conventional hot-pressing and

subsequent deformation processes.

To sum up, the heat-resistant Al materials mentioned above all face the risk of losing strengthening efficacy at high temperatures, that is to say, when the preparation/service condition exceeds a critical temperature for a certain time, a permanent damage in strength will be resulted. Therefore, developing thermally stable Al materials is still an open question.

Recently, Al<sub>2</sub>O<sub>3</sub>/Al composites fabricated from ultrafine Al powders were reported to exhibit superior mechanical properties at elevated temperatures [12–14]. The lamellar nanometric amorphous Al<sub>2</sub>O<sub>3</sub> (am-Al<sub>2</sub>O<sub>3</sub>) distributed at the Al grain boundaries (GBs) can stabilize the microstructure and enhance the strength effectively. High-temperature strength can be enhanced by a small volume fraction of Al<sub>2</sub>O<sub>3</sub>, and therefore, sufficient deformation ability can be preserved [12,14]. However, it was reported that the lamellar am-Al<sub>2</sub>O<sub>3</sub> would transformed into granular γ-Al<sub>2</sub>O<sub>3</sub> at temperatures above 450 °C, resulting in serious strength reduction [13,15]. This critical temperature also brings formidable difficulties to conventional hot-pressing fabrication and deformation of the Al<sub>2</sub>O<sub>3</sub>/Al composites.

\* Corresponding author.

\*\* Corresponding author.

E-mail addresses: [blxiao@imr.ac.cn](mailto:blxiao@imr.ac.cn) (B.L. Xiao), [zym@imr.ac.cn](mailto:zym@imr.ac.cn) (Z.Y. Ma).

<sup>1</sup> These authors contributed equally to this work.

The crystallization of am- $\text{Al}_2\text{O}_3$  on Al powders is decided by both thermodynamics and kinetics processes [16–18]. Firstly, the thermodynamic factors are considered. Compared to  $\gamma$ - $\text{Al}_2\text{O}_3$ , the higher bulk Gibbs free energy of am- $\text{Al}_2\text{O}_3$  can be compensated by the lower sum of its surface and interfacial energies until the thickness of am- $\text{Al}_2\text{O}_3$  reaches a certain value. Therefore, a critical oxide-film thickness exists for the thermodynamic stability of am- $\text{Al}_2\text{O}_3$ . The thinner it is, the more stable am- $\text{Al}_2\text{O}_3$  will be [16,17,19]. Secondly, the kinetic factors are taken into account. For am- $\text{Al}_2\text{O}_3$  in almost oxygen-free environments (hot-pressing or annealing processes), with the increase of temperature, the thickness of partial am- $\text{Al}_2\text{O}_3$  increases as the result of enhanced mobility of the oxygen species [18] and Al atoms [20,21], which lowers the energy barrier of nucleation of  $\gamma$ - $\text{Al}_2\text{O}_3$ . Therefore, the avoidance of crystallization of am- $\text{Al}_2\text{O}_3$  should consider both thermodynamics and kinetics processes. However, because of the difficulty in regulating or decorating the 2D am- $\text{Al}_2\text{O}_3$ , to the best of our knowledge, no feasible solution has been proposed.

Graphene, a kind of 2D material with the excellent strength, high Young's modulus and low density, is regarded as potential candidate for reinforcements of metal matrix composites [22–24]. Some chemical methods, such as chemical vapor deposition and molecular-level mixing have been applied to introduce graphene into metal matrix [25,26]. However, these methods are not suitable for Al matrix. The extremely large specific surface area brings restrictions in additive amount [27–29], and thus, the overall strengthening effect of graphene sheets is hard to reach a value comparable with other conventional reinforcements [30]. Furthermore, the addition of graphene often results in significant decrease in the ductility of the composites [31–36]. Therefore, the application of graphene as the reinforcement in Al matrix composites (AMCs) is still in the developing stage.

Considering the 2D morphology of graphene, it is highly possible to use graphene to decorate the lamellar am- $\text{Al}_2\text{O}_3$ , thereby stabilizing the thermal stability of am- $\text{Al}_2\text{O}_3$ . In previous studies, it is reported that graphene (reduced graphene oxide (rGO)) can be introduced by the electrostatic interaction between graphene oxide (GO) and Al powders, and the following thermal reduction process [33,37]. By this mean, rGO can be successfully introduced on spherical and flaky Al powders [33, 37]. However, no study on ultrafine Al powders has been reported, to the best of our knowledge.

In this study, rGO sheets were applied for the first time to enhance high-temperature strength of  $\text{Al}_2\text{O}_3/\text{Al}$  composites compacted from ultrafine Al powders (1.45  $\mu\text{m}$ ), and microstructure and mechanical properties of the composites were investigated. The aims of this study are (a) to verify the feasibility of introducing rGO to decorate the lamellar am- $\text{Al}_2\text{O}_3$  in the  $\text{Al}_2\text{O}_3/\text{Al}$  composites, (b) to enhance the high-temperature strength of the composites, and (c) to elucidate the mechanism of rGO in stabilizing the lamellar am- $\text{Al}_2\text{O}_3$ .

## 2. Experimental procedure

### 2.1. Preparation of GO colloid

GO colloid was prepared using the modified Hummers method. Chemicals were bought from Sinopharm Chemical Reagent Co.. The detailed fabrication procedure was based on Ref. [38]. Finally, GO dispersion with the concentration of 6 mg/ml was obtained.

### 2.2. Preparation of rGO/Al composites

Commercial Al powders with an average diameter of 1.45  $\mu\text{m}$  purchased from Angang Group Aluminum Powder Co. were used. The mixture of GO/Al powders was prepared via the electrostatic adsorption between GO and Al powders [39]. First, GO colloid was diluted and ultra-sonicated, until GO dispersion with a concentration of 2 mg/ml was obtained. Second, 200 g Al powders were dispersed uniformly in 200 g alcohol by mechanical stirring. Third, GO dispersion was poured

in directly, and the slurry was stirred until the finish of adsorption. Finally, the slurry was filtered, rinsed and dried at 60 °C for 12 h, and GO/Al powders with the GO concentration of 0.2 wt% (abbreviated Sample 0.2), 0.6 wt% (abbreviated Sample 0.6) and 1.0 wt% (abbreviated Sample 1.0) were obtained.

GO/Al powders were annealed in a furnace of Ar atmosphere at 500 °C for 2 h to reduce GO sheets. Then powder metallurgy technique was applied to fabricate the composites. The mixture powders were first cold pressed under a pressure of 70 MPa. Then hot pressing was carried out in a vacuum chamber of  $10^{-2}$  Pa. Temperature was raised to 600 °C and kept for 2 h, after which a pressure of 50 MPa was used to realize densification. In the hot-pressing procedure, GO could be more sufficiently reduced. Finally, extrusion with an extrusion ratio of 16:1 was performed at 450 °C.

For comparison, Al powders without adsorbed GO sheets were also compacted after being treated using the same processes as the rGO/Al composites. The same hot-pressing temperature of 600 °C was used to verify the effects of rGO addition (abbreviated Sample 0).

### 2.3. Characterization

Al powders were observed using scanning electron microscopy (SEM, Leo Supra 55). GO sheets were observed using atomic force microscope (AFM) and SEM. X-ray diffractometer (XRD, D-MAX/2400 using Cu K $\alpha$  radiation) and Raman spectroscopy were used to analyse the composition of the composites. GO colloid was filtered, rinsed and dried at 60 °C for 12 h, then subjected to thermal analyses to examine the heating-driven reduction process of GO sheets by TG-DSC using STA 449C Jupiter under argon atmosphere. The chemical composition of GO was characterized by X-ray photoelectron spectroscopy (XPS) on ESCA-LAB250 using Al K $\alpha$  radiation, and spectra was calibrated to the binding energy of C=C bonds (284.6 eV). Microstructure characterizations of the composites were carried out by transmission electron microscopy (TEM, FEI Tecnai F30). TEM specimens were prepared by grinding and dimpling, followed by milling (Gatan PIPS, Model 695).

### 2.4. Mechanical property test

Tensile specimens with a gauge length of 25 mm, a diameter of 5 mm were machined parallel to the extrusion direction. Tensile test was carried out at both RT and 350 °C using Instron 5582 tester. A strain rate of  $1 \times 10^{-3} \text{ s}^{-1}$  was used. At least 3 tensile specimens were tested for each sample.

## 3. Results

### 3.1. Characterization of the GO/Al powders

Fig. 1a and b show SEM images of as-received ultrafine Al powders and sonicated GO sheets, respectively. Although GO sheets were easily dispersed in water, they would be reagglomerated if the size is much larger than that of Al powders [39]. On the other hand, too small GO sheets are disadvantageous to the strengthening effect according to load-transfer strengthening theory [40]. Therefore, it is considered that an optimized size coordination of Al powders and GO sheets can be realized if the size of GO sheets is equivalent to the diameter of aluminum powders. From Fig. 1a and b, it can be seen that the size of GO sheets and Al powders was close. In Fig. 1c, the AFM image shows that GO sheets exhibited a thickness of about 1 nm, corresponding to the single-layer GO [41]. Obviously, the good dispersibility of GO was observed, attributable to the abundant hydrophilic oxygen containing groups.

The chemical composition and bonding states of GO were examined by XPS and the results are shown in Fig. 2a. The C/O ratio of GO was about 1.6. The C 1s spectrum of GO can be fitted into three peaks at binding energies of 284.6 eV for  $\text{sp}^2 \text{C}=\text{C}$  (graphite carbon), 286.6 eV

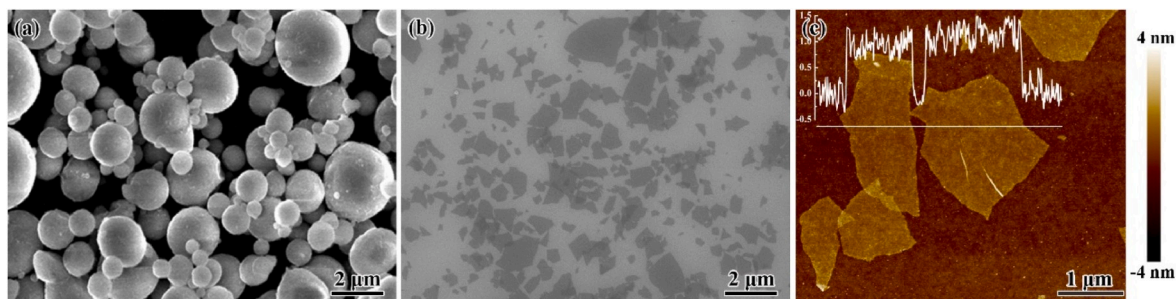


Fig. 1. SEM images of (a) ultrafine Al powders, (b) SEM and (c) AFM images of GO sheets.

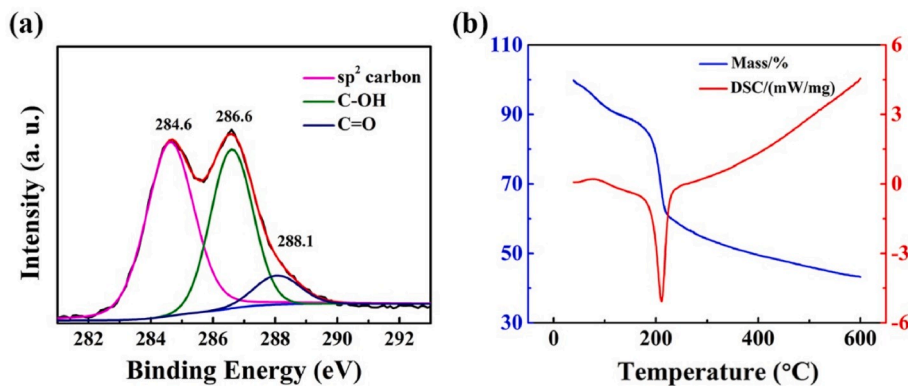


Fig. 2. (a) XPS and (b) TG-DSC curves of GO sheets.

for C–O (hydroxyl and epoxide groups) and 288.1 eV for C=O (carbonyl groups). Thermal analyses were conducted to study the heating-driven changes of GO powders and the results are shown in Fig. 2b. For GO nanosheets, the first-stage mass-loss at about 100 °C reflects the loss of intercalated adsorbent water molecules among interlayers, corresponding to an endothermic DSC signal [42]. The abrupt mass-loss and the exothermic DSC signal at a narrow temperature range (150–250 °C) illustrate that most of oxygen-containing groups bonded to graphene planes were removed. Finally, about 57% of the original mass was lost in total, which means that the mass fractions of rGO in Samples 0.2, 0.6 and 1.0 were 0.086%, 0.258% and 0.43%, respectively.

Fig. 3a–c shows representative SEM images of Al powders after adsorption of 0.2 wt%, 0.6 wt% and 1.0 wt% GO sheets. The darker region corresponds to adsorbed GO sheets. It can be seen that coverage ratio of GO sheets on the Al powders increased with increasing the weight percentage of GO. An excessive coverage of GO sheets was observed in Sample 1.0 with 1.0 wt% GO sheets (Fig. 3c).

### 3.2. Microstructure of the composites

Density values of the as-extruded composites are given in Table 1. In

previous studies, the difference in density of am-Al<sub>2</sub>O<sub>3</sub> and Al is usually neglected because the values are close [12,13,43]. Though error might exist, from Table 1, it can be seen that the density of Sample 1.0 is over 99.4% of that of Sample 0. It indicates that in spite of the hindering effects of rGO, full density could be obtained for the composites with rGO addition after sintering and extrusion.

XRD patterns of the as-extruded composites are shown in Fig. 4a. Al<sub>4</sub>C<sub>3</sub> is commonly formed in graphene reinforced Al matrix composites during ball-milling and hot-pressing process [45,46]. However, in this study, for all of the composites fabricated, only Al peaks can be observed. Even in the magnified view (inset in Fig. 4a), the strongest

Table 1

Density of composites with various rGO concentrations (The densities of r-GO and Al were taken as 2.0 g/cm<sup>3</sup> and 2.7 g/cm<sup>3</sup>, respectively [44]).

Sample	rGO content (vol%)	Measured density (g/cm <sup>3</sup> )	Relative density (%)
0	0	2.705	100.2
0.2	0.102	2.697	99.9
0.6	0.305	2.688	99.6
1.0	0.509	2.689	99.7

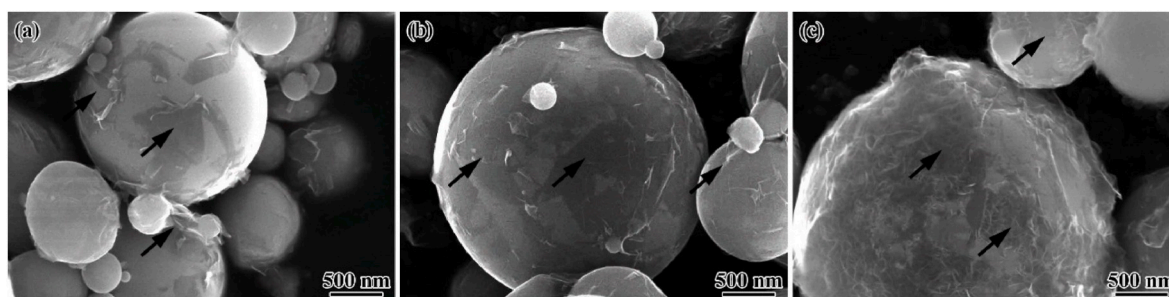


Fig. 3. SEM images of GO/Al powders with the GO (black arrows) concentration of (a) 0.2 wt%, (b) 0.6 wt% and (c) 1.0 wt%.

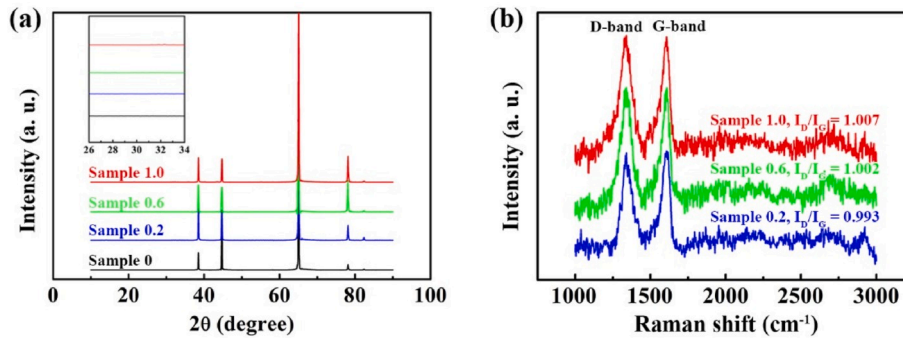


Fig. 4. (a) XRD patterns and (b) Raman spectra of the composites.

peak of  $\text{Al}_4\text{C}_3$  ( $\sim 31^\circ$ ) cannot be detected. It indicates that almost no  $\text{Al}_4\text{C}_3$  was produced in the preparation process, which can be attributed to the moderate preparation process, and the obstruction effect of am- $\text{Al}_2\text{O}_3$  between Al and rGO. Because of the small quantity ( $\leq 0.43$  wt %) and few layers of rGO, the broad peak of rGO was not detected by XRD, and the same phenomenon was also found in Refs. [44,46,47].

Raman spectrum can be used to reveal the structure and defects of graphene [31], and higher  $I_D/I_G$  value indicates more defects in graphene [45]. As shown in Fig. 4b, the  $I_D/I_G$  ratios of the composites in the present study exhibit a value of  $\sim 1.0$ , which are much lower than that of composites fabricated by other preparation methods such as ball-milling [31,45]. The results of XRD patterns and Raman spectra confirmed the feasibility of the fabrication process in the present study.

Fig. 5a–d shows the grain structure of Samples 0, 0.2, 0.6 and 1.0, respectively. The average grain sizes of the composites were obtained by counting over 200 grains for each composite. The average grain size was 760, 460, 285 and 395 nm, respectively, for Samples 0, 0.2, 0.6 and 1.0. It was shown that the addition of rGO caused obvious grain refining of Al matrix. The grain size first decreased and then increased a bit with increasing the rGO concentration, and the reasons will be discussed in Section 4.1. Furthermore, compared with Samples 0 and 0.2, darker contrast was shown in Samples 0.6 and 1.0, and more dislocations were observed in the grains (inset in Fig. 5c), indicating higher strain and

more dislocation accumulation.

For Sample 0 without rGO addition, clean coarser grains with particles distributed mainly at the GBs can be observed (Fig. 6a). High resolution TEM image and its Fast Fourier Transform (FFT) pattern are inserted in Fig. 6a. The FFT pattern could be indexed by the [110] zone-axis of an fcc lattice with a lattice parameter  $a = 7.93$  nm. This suggests that the aluminium oxide particle was  $\gamma\text{-Al}_2\text{O}_3$  (space group Fd3m). It is considered that at high pressing temperature of  $600^\circ\text{C}$ , am- $\text{Al}_2\text{O}_3$  first became thicker by diffusion and reached a certain critical thickness, then higher bulk Gibbs free energy prompted the transformation of am- $\text{Al}_2\text{O}_3$  into  $\gamma\text{-Al}_2\text{O}_3$  [17].

In Fig. 6b–d, rGO in the Al matrix was disclosed by under focus or over focus for its clear exhibition (the locations of rGO are denoted by white arrows). In Sample 0.2 (Fig. 6b), relatively clean grains with well dispersed rGO at the GBs were observed. The amount of  $\gamma\text{-Al}_2\text{O}_3$  was much smaller compared to that in Sample 0. As shown in Fig. 6c, more rGO sheets were observed in Sample 0.6, exhibiting a well dispersion at the GBs and a reticular distribution. Finer grains with more strain were disclosed. It was also observed that most of the rGO sheets were distributed at the GBs. With increasing the original GO concentration to 1.0 wt%, almost all the GBs were decorated with rGO. Clusters were also observed, being consistent with SEM observation as shown in Fig. 3c.

RGO sheets in Sample 0.2 are shown in Fig. 7a, and some regions

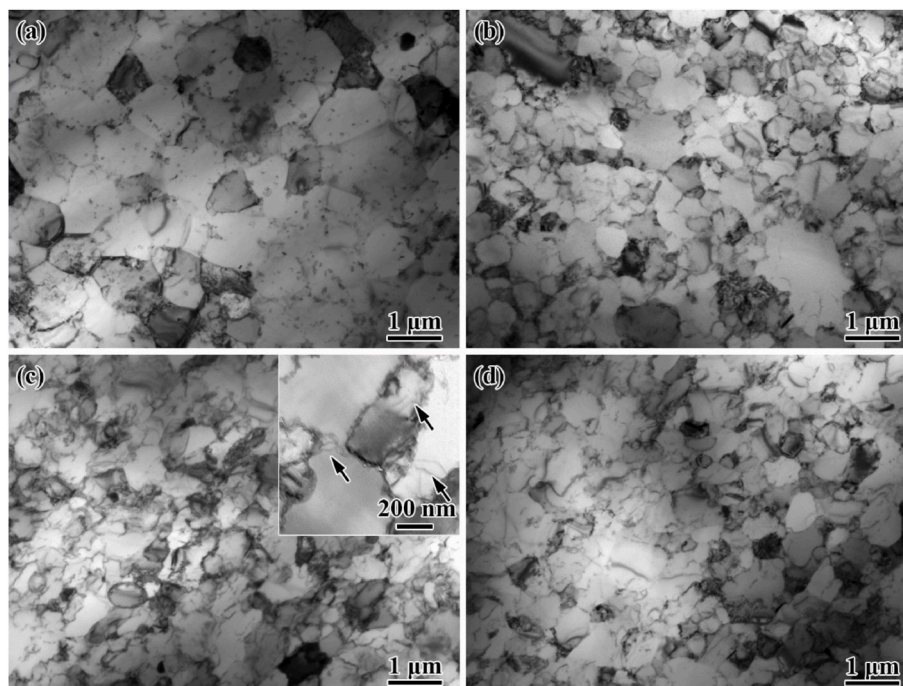
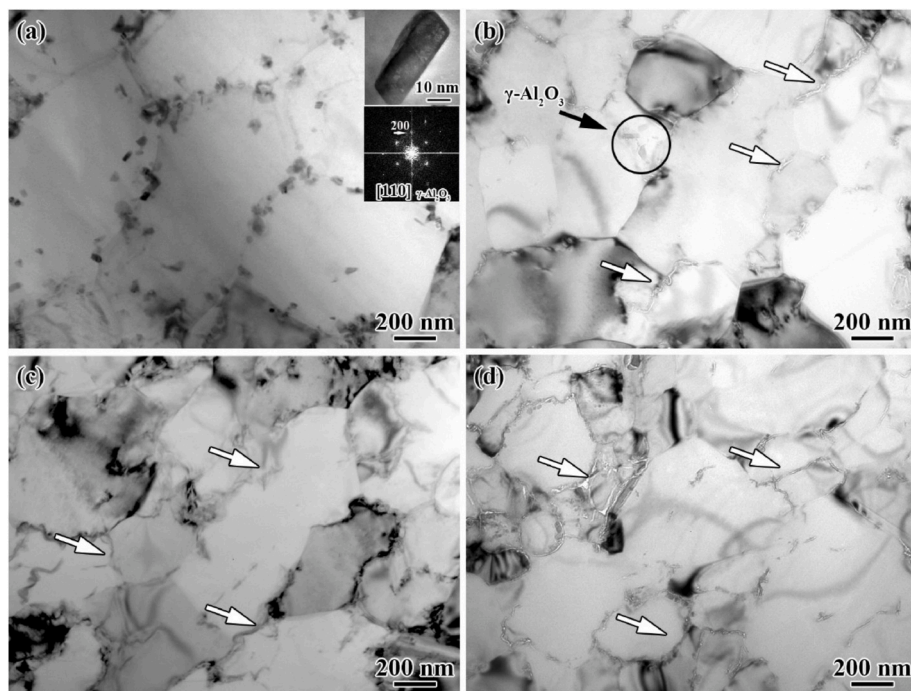


Fig. 5. TEM images showing grain structure of Samples (a) 0, (b) 0.2, (c) 0.6 and (d) 1.0 (Dislocations are indicated by black arrows).



**Fig. 6.** TEM images showing  $\text{Al}_2\text{O}_3$  and rGO in Samples (a) 0, (b) 0.2, (c) 0.6 and (d) 1.0 ( $\gamma\text{-Al}_2\text{O}_3$  is indicated by black arrows and circle, and rGO is indicated by white arrows).

were magnified to show the details (Fig. 7b–d). Unlike the Al GB without rGO sheets as shown in Fig. 7b, rGO sheets with about 5 layers can be clearly seen in Fig. 7c and d, with two amorphous layers on the both sides of rGO sheets. Considering the smaller amount of  $\gamma\text{-Al}_2\text{O}_3$  in Samples 0.2, 0.6 and 1.0 than that in Sample 0, it is reasonable to speculate that the amorphous layers corresponded to the am- $\text{Al}_2\text{O}_3$  that had not transformed into  $\gamma\text{-Al}_2\text{O}_3$ .

A TEM image of Sample 0.2 and its corresponding HAADF image are

shown in Fig. 8a and b. In the HAADF mode, bright contrast indicates the existence of heavy atoms or constituents with higher density [48], so rGO sheets in the Al matrix exhibit dark contrast. It was found that almost all the dark-contrast sheets were accompanied by some adjoining bright contrast, corresponding to the amorphous layers as shown in Fig. 7d. By EDS elemental analysis and mapping as shown by the insets in Fig. 8b, O element concentration was revealed. Since most of oxygen containing groups in GO sheets had been removed by reduction, it can be

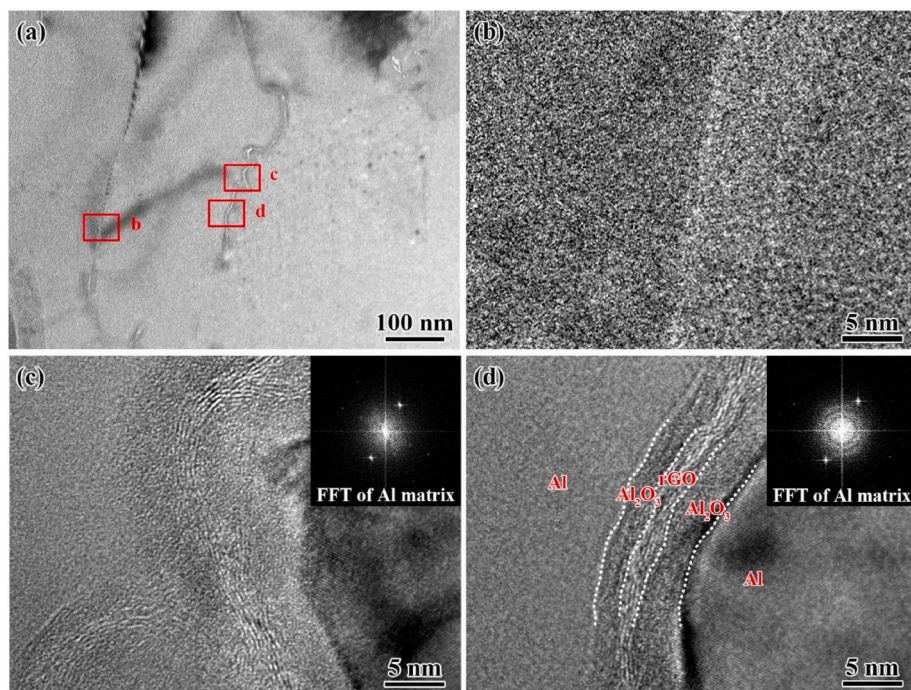


**Fig. 7.** (a) TEM image of Sample 0.2, and magnified views of selected areas in red rectangles are shown in (b), (c), and (d), respectively. (For interpretation of the references to colour in this figure legend, the reader is referred to the Web version of this article.)

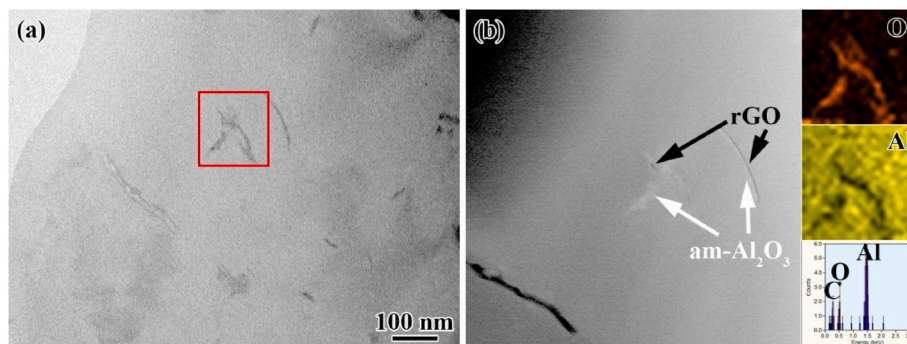


**Fig. 8.** (a) A TEM image of Sample 0.2 and (b) corresponding HAADF image with EDS elemental analysis of selected area in red rectangle. (For interpretation of the references to colour in this figure legend, the reader is referred to the Web version of this article.)

confirmed that the amorphous layers shown in Fig. 7d were oxygen-rich. Thus, it was verified that the amorphous layers were am- $\text{Al}_2\text{O}_3$  reserved in the composites, even if the hot-pressing was carried out at the same high temperature of 600 °C as Sample 0.

High resolution TEM images of rGO sheets in Sample 1.0 are shown in Fig. 9. Because of excess addition, rGO sheets with overmuch layers were piled-up in the adsorption process with a roughly parallel distribution, as shown in Fig. 9a. In Fig. 9b, a rolled-up morphology of the rGO sheets was also revealed, which could not be formed in the processes from adsorption to hot-pressing of GO sheets. It is believed that in the extrusion process, with the GB sliding (GBS) of the Al matrix, rGO sheets were twisted and folded.

### 3.3. Mechanical properties

Fig. 10 shows the tensile stress–strain curves of the composites, and tensile properties are listed in Table 2. It is shown that compared to Sample 0, the strengths of Samples 0.2, 0.6 and 1.0 were significantly increased due to the addition of rGO. At both RT and 350 °C, with increasing the addition amount of rGO the strength of the composites increased first and then decreased and the reasons will be discussed in Section 4.3. Sample 0.6 with the addition of only 0.305 vol% rGO exhibited the highest tensile strength (241 MPa at RT and 129 MPa at 350 °C) among the composites. Strength enhancement of 65% and 121% was realized respectively.

Some representative study results from other researchers are listed in Table 3. In graphene/Al composites fabricated by ball-milling, the strength of the composite was enhanced by fine-grain strengthening caused by ball-milling process, and the strengthening efficiency of graphene (strength enhancement ratio caused by graphene addition of each volume percent) was 46% [28]. The flake-powder strategy was applied in Ref. [33,35]. Compared to their control samples fabricated by flake powders without rGO addition, the strengthening efficiency of rGO was lower than 40%. The strengthening efficiency values were relatively

lower, because the thick  $\text{Al}_2\text{O}_3$  films (about 10 nm in thickness) resulting from ball-milling process is more stable at high temperature and hard to sinter [49], which restricted the strengthening effect of rGO. Also, deformability of the composite was restrained. In Refs. [47], spherical powders with an average diameter of 5.5  $\mu\text{m}$  were used to adsorb GO sheets. Spark plasma sintering was used, thus, am- $\text{Al}_2\text{O}_3$  could remain in both experimental and control samples due to short high-temperature residence time. The original am- $\text{Al}_2\text{O}_3$  on spherical powders was more deformable, therefore, the ductility could be higher, and strengthening efficiency of rGO reached a value of 120%.

In the present study, ordinary vacuum hot-pressing which is more preferable for engineering application was used. Am- $\text{Al}_2\text{O}_3$  was transformed into  $\gamma\text{-Al}_2\text{O}_3$  in control sample. In Sample 0.6, a strengthening efficiency up to 213% was obtained, attributing to direct strengthening effect of rGO and its stabilization effect on am- $\text{Al}_2\text{O}_3$ . More notably, at 350 °C, the first attempt, to the best of our knowledge, to enhance the high-temperature strength of AMCs using rGO sheets was confirmed to achieve significant effect. Significant strengthening efficiency of GB-distributed (am- $\text{Al}_2\text{O}_3$ +rGO) in Sample 0.6 was as high as 396%, which confirmed a more enormous application potential of rGO in developing heat-resistant AMCs.

### 3.4. Fractographs

SEM images of the RT fracture surfaces of Samples 0, 0.6 and 1.0 are shown in Fig. 11. It was found that dimples in Samples 0.6 and 1.0 were smaller than those in Sample 0, indicating decreased ductility of the composites. On the fracture surface of Sample 0.6 with a higher magnification (inset in Fig. 11b), rGO sheets could be observed with most of them in the bottom of the dimples, which is in accord with the microvoid coalescence fracture mode.

When testing temperature increased to 350 °C, obvious intergranular fracture was observed in these composites (Fig. 12). Fractographs of Samples 0.6 and 1.0 exhibited a finer morphology (Fig. 12b and c) than

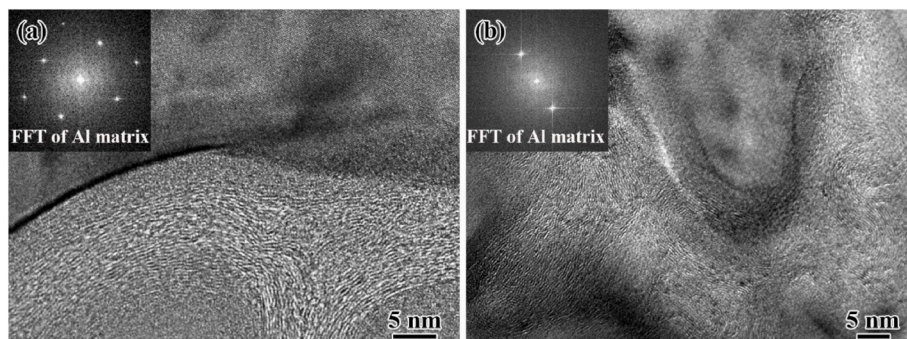


**Fig. 9.** High resolution TEM images showing rGO sheets in Sample 1.0 with (a) parallel and (b) rolled-up morphology.

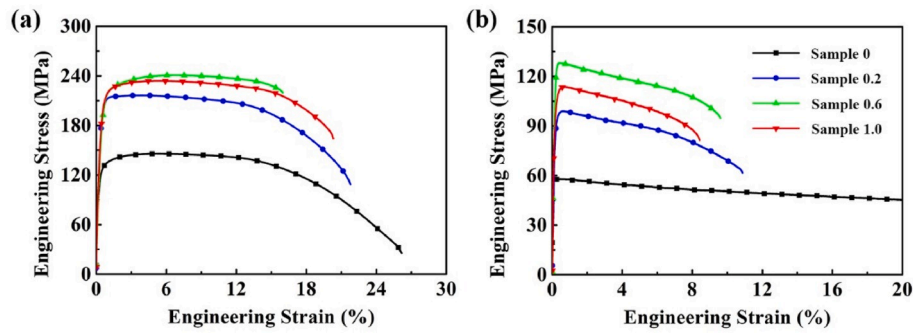


Fig. 10. Tensile stress-strain curves for various composites at (a) RT and (b) 350 °C.

Table 2

Tensile properties of the composites with various rGO concentrations.

Sample	rGO (vol%)	Layer of rGO <sup>a</sup>	RT			350 °C		
			YS (MPa)	UTS (MPa)	El (%)	YS (MPa)	UTS (MPa)	El (%)
0	0	0	116	146	26	55	58	35
0.2	0.102	~1	183	216	22	91	99	11
0.6	0.305	~4	207	241	16	121	128	10
1.0	0.509	~7	206	234	20	109	114	9

YS: Yield strength, UTS: Ultimate tensile strength and El: elongation.

<sup>a</sup> Layers of rGO in various composites were calculated in Section 4.1.

Table 3

Comparison in mechanical properties of various rGO/Al composites fabricated with different raw materials.

rGO (vol %)	UTS (MPa)	El. (%)	Temperature	Strengthening efficiency (%) <sup>a</sup>	Ref.
0.500	287	17	RT	46	[28]
1.500	302	3	RT	33	[33]
2.600	318	3	RT	38	[35]
0.250	178	19	RT	120	[47]
0.305	241	16	RT	213	This study
0.305	128	10	350 °C	396	This study

UTS: Ultimate tensile strength. El.: Elongation.

<sup>a</sup> Strength enhancement rate caused by rGO addition of each volume percent.

that of Sample 0 (Fig. 12a), in accordance with the finer grain structure shown in TEM observation (Fig. 5). On the fracture surface of Sample 0.6 with a higher magnification (inset in Fig. 12b), rGO sheets were observed. However, the pull-out length of the rGO sheets on the fracture surfaces at 350 °C was reduced compared to that at RT as shown in Fig. 11c. Therefore, it can be concluded that fracture mode at 350 °C changed into grain boundary damage.

## 4. Discussion

### 4.1. Microstructure

In water, Al powders are ionized, producing  $Al^{3+}$  ( $Al = Al^{3+} + 3e^{-}$ ).  $Al^{3+}$  attaching to the Al powder surface made negatively charged GO sheets adsorbed on the Al powders [39]. Therefore, tight coupling between Al and GO could be formed in the mixing process via the electrostatic attraction force, thus reagglomeration could be avoided in the following processes.

The numbers of rGO layers in different composites can be calculated using its thickness and the diameter of Al powders. In the critical condition that single-layered GO covers the Al powders, taking the thickness of GO as 1 nm and the diameter of Al powders as 1.45  $\mu m$ , the volume fraction of GO can be calculated as  $1 - (1450/1452)^3 = 0.41\%$ . Using the density of approximately 2.0  $g/cm^3$  and 2.7  $g/cm^3$  for GO and Al [44], the weight percentage in this critical condition is 0.30%. That is to say, according to theoretical calculation, the weight percentage of single-layer GO covering fully on the Al powder surface is 0.3 wt%.

Being consistent with the calculation above, as shown in Fig. 3, GO sheets with concentration lower than 0.3 wt% were not enough to fully cover the Al powder surface. Furthermore, considering the two bonded adjacent Al powders, the average layer number of rGO in Samples 0.2, 0.6 and 1.0 is calculated to be 1, 4, and 7, respectively, as listed in Table 2.

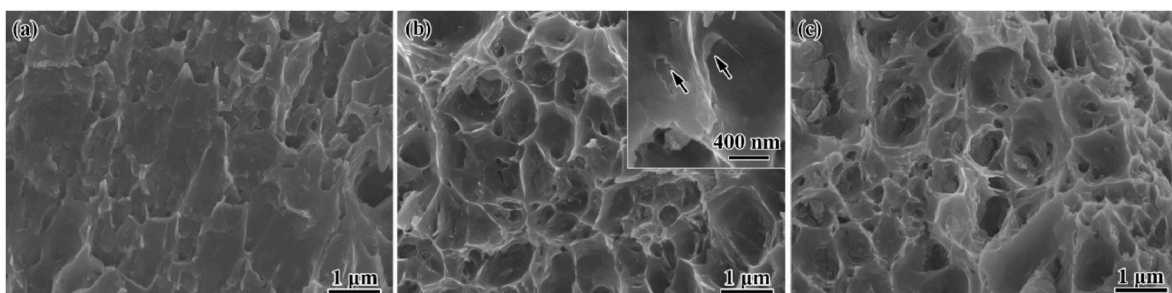


Fig. 11. SEM fractographs of Samples (a) 0, (b) 0.6 (the inset is the magnified view showing rGO sheets) and (c) 1.0 at RT (rGO sheets are indicated by black arrows).

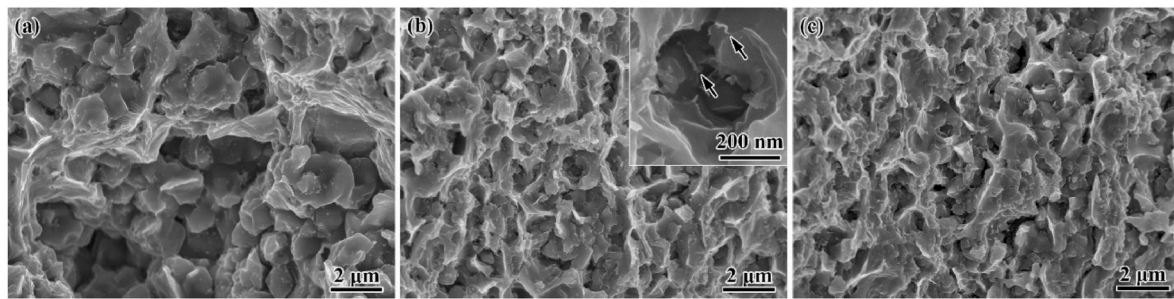


Fig. 12. SEM fractographs of Samples (a) 0, (b) 0.6 (the inset is the magnified view showing rGO sheets) and (c) 1.0 at 350 °C (rGO sheets are indicated by black arrows).

During an extrusion process, the Al grains were refined by dynamic recrystallization [50]. Dislocation walls and dislocation cells would first form and then develop into low angle grain boundaries and subgrains. Low angle grain boundaries could be finally transformed into high angle grain boundaries, resulting in fine grain structure [50,51]. In this process, the nanosized reinforcements in the Al matrix could promote generation of dislocations and limit their slip, thereby finer grains could be obtained by dynamic recrystallization. On the other hand, nanosized reinforcements could further stabilize the GBs and prevent the grains from coarsening. As a result, grain refinement was greatly promoted by the reinforcements (rGO and am-Al<sub>2</sub>O<sub>3</sub> in this study) [51–53].

For Sample 0, the lamellar am-Al<sub>2</sub>O<sub>3</sub> distributed at the GBs was transformed into the granular  $\gamma$ -Al<sub>2</sub>O<sub>3</sub> in the hot-pressing process, resulting in significantly reduced GB pinning effect [15]. When rGO was introduced in the Al matrix, the GB-distributed reinforcements (am-Al<sub>2</sub>O<sub>3</sub>+rGO) restricted the mobility of the GBs [4]. More lattice strain and dislocations was produced, and therefore the driving force for dynamic recrystallization increased. It can be confirmed from Figs. 5 and 6 that the strain and dislocation accumulation in Samples 0.6 and 1.0 were higher than those in Samples 0 and 0.2. As a result, the grain sizes in Sample 0, 0.2 and 0.6 decreased with the increase of rGO concentration.

However, when the initial GO concentration increased to 1.0 wt%, the grain size increased. It was reported that friction force between graphene sheets was affected by the number of graphene layers and the friction decreased with the increase of layer number [54–56]. When graphene layers were more than 5 layers, the friction force could exhibit the similar low value of bulk graphite [57,58] that is often used for lubrication. According to our calculated results (Table 2), when 1.0 wt% GO was introduced into the Al matrix, the layer number of rGO was 7 averagely and the friction force between sheets decreased, so the GB pinning effect became much weaker. GBs and deformation could be freer, so lattice strain and dislocations were less, and the grains in Sample 1.0 were a little coarser than those in Sample 0.6.

#### 4.2. Enhanced thermal stability of am-Al<sub>2</sub>O<sub>3</sub>

During the hot-pressing process, the lamellar am-Al<sub>2</sub>O<sub>3</sub> in Sample 0 was transformed into the granular  $\gamma$ -Al<sub>2</sub>O<sub>3</sub>. For Samples 0.2, 0.6 and 1.0, although composites were hot-pressed at the same temperature of 600 °C, the lamellar am-Al<sub>2</sub>O<sub>3</sub> was well preserved (Fig. 6). The enhanced thermal stability can be explained by thermodynamics and kinetics:

(1) Thermodynamic. To finish the crystallization, the decrease in bulk Gibbs free energy must be higher than the increase in surface and interfacial energies. Thus, the thickness of am-Al<sub>2</sub>O<sub>3</sub> must become larger than the critical value [16,17]. When two Al powders were sintered together, the am-Al<sub>2</sub>O<sub>3</sub> on their surfaces was bonded together, therefore, the thickness of Al<sub>2</sub>O<sub>3</sub> doubled, making it more liable to transform [13]. It is comprehensible that when rGO sheets were introduced within the Al powders, the thickness of the am-Al<sub>2</sub>O<sub>3</sub> can be halved, so the am-Al<sub>2</sub>O<sub>3</sub> can be more thermally stable.

(2) Kinetic. Since there was almost no oxygen during the hot-pressing

process, the thickening of am-Al<sub>2</sub>O<sub>3</sub> depended on diffusion of the oxygen species and Al atoms [18,20,21]. First, rGO sheets within the am-Al<sub>2</sub>O<sub>3</sub> layers could block the diffusion as physical barrier. Second, GO sheets and Al powders could transfer electrons and form interaction forces between them during the adsorption process, which could further hinder the diffusion. Thus, the Ostwald ripening process and transformation of am-Al<sub>2</sub>O<sub>3</sub> were held back.

#### 4.3. Enhanced strength

At RT, the strength of the composites fabricated in this study depends mainly on their grain size and rGO addition. For the Al matrix, considering the Hall–Petch strengthening, finer grains can result in higher strength [30]. Furthermore, as the consequence of rGO addition, the (am-Al<sub>2</sub>O<sub>3</sub>+rGO) could enhance the strength effectively by load-transfer strengthening. Therefore, with the concentration of GO increasing from 0.2 wt% to 0.6 wt%, the finer grain size and stronger load-transfer strengthening resulted in the higher RT strength. When the GO concentration increased further to 1.0 wt%, the grain size of Sample 1.0 became coarser and the strengthening effect of rGO was also weakened because of agglomeration, so the RT strength became lower. However, sample 1.0 with coarser grains exhibited the increased elongation due to increased strain hardening capability.

At high temperatures, the GBs lost their strength and became the weak spot of the composites [15,59]. Without being pinned, GBs could slide easily at high temperature, and dislocations could easily annihilate in the tensile process at the GBs by dynamic recovery. As shown in Fig. 13a, the GBs were almost free of particles in Sample 0 after tensile testing at 350 °C, which was obviously different from the as-extruded state (Fig. 6a), indicating that obvious boundary sliding/migration happened during the tensile process because of weak GB pinning effect of  $\gamma$ -Al<sub>2</sub>O<sub>3</sub> [60]. It could be also seen from the clean GBs that the GBs hardly exhibited dislocation impediment effect in Sample 0. Only a few of dislocations were pinned by  $\gamma$ -Al<sub>2</sub>O<sub>3</sub>.

Microstructure of Sample 0.6 after tensile testing at 350 °C is shown in Fig. 13b. The (am-Al<sub>2</sub>O<sub>3</sub>+rGO) could strengthen the GBs and pin them against sliding, therefore, the microstructure was quite stable and dark contrast was observed near the GBs, indicating dislocation accumulation [49]. As shown in Fig. 13c, although no particles existed in the Al grains, dislocation accumulation could form in the Al grains. This confirmed that (am-Al<sub>2</sub>O<sub>3</sub>+rGO) located at the Al grain boundaries could improve the stability of the grain boundaries and strongly hindered dislocation annihilation, resulting in higher high-temperature strength.

Therefore, the (am-Al<sub>2</sub>O<sub>3</sub>+rGO) could enhance the high-temperature strength significantly. However, for Sample 1.0, the friction force between rGO sheets declined due to the excessive layer number as discussed in Section 4.1, so the GB pinning effect was weakened and the high-temperature strength of composite decreased. The inevitable softening and recovery behavior at the GBs could lead to localized deformation and provoke voids and fracture, so intergranular fracture happened at high temperature for all the composites [4,60]. Clusters of

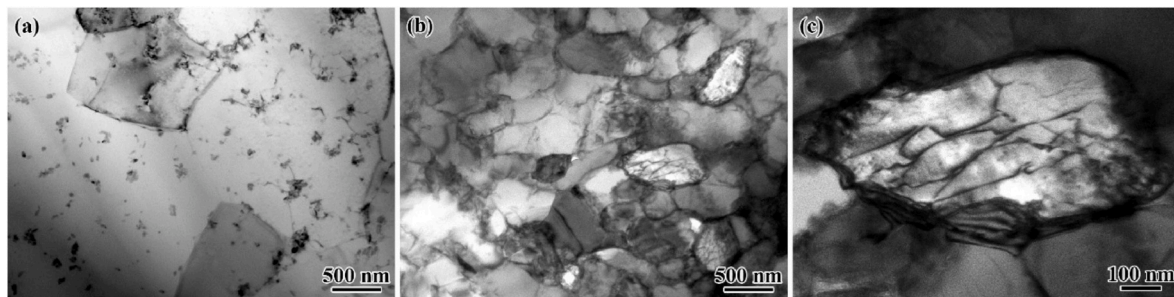


Fig. 13. TEM images showing microstructure in Samples (a) 0 and (b) 0.6, and (c) dislocations in sample 0.6 after tensile testing at 350 °C.

rGO at the Al GBs in Sample 1.0 aggravated the discordance at the GBs, so intergranular fracture happened earlier in Sample 1.0, resulting lower elongation.

The overall implication of the experimental results is significant. It was confirmed that graphene exhibited great application foreground and the strengthening effect is expected to be further utilized in fabricating high-temperature Al materials. For further increasing the properties, finer Al powders can be used to obtain higher strength by introducing more reinforcements in the future study.

## 5. Conclusions

- (1) Reduced graphene oxide (rGO) sheets were introduced into  $\text{Al}_2\text{O}_3/\text{Al}$  composites via electrostatic interaction between GO and ultrafine Al powders. Well dispersion of rGO could be realized until the original GO concentration increased to 1.0 wt%.
- (2) rGO sheets could stabilize the amorphous  $\text{Al}_2\text{O}_3$  (am- $\text{Al}_2\text{O}_3$ ) and prevent it from transforming into  $\gamma\text{-Al}_2\text{O}_3$  during the hot-pressing process, which could be explained by thermodynamics and kinetics factors. Lamellar (am- $\text{Al}_2\text{O}_3$ +rGO) distributed at the grain boundaries (GBs) exhibited a reticular distribution.
- (3) Strength at both room and high temperatures could be increased significantly with addition of a very small number of rGO because of both direct strengthening effect of rGO and its stabilization effect on am- $\text{Al}_2\text{O}_3$ . With addition of 0.305 vol% rGO, strength enhancement of 65% and 121% was realized at room temperature and 350 °C, respectively.
- (4) (am- $\text{Al}_2\text{O}_3$ +rGO) could refine the Al grains and stabilize the GBs. Compared to the composite without rGO addition, at RT, both the grain-refining and load-transfer strengthening mechanisms could contribute to higher strength; at high temperature, the GB pinning effect of (am- $\text{Al}_2\text{O}_3$ +rGO) could lead to higher strength.

## Data availability

The raw/processed data will be made available on request.

## Declaration of competing interest

The author declares that they have no known competing financial interests or personal relationships that could have appeared to influence the work reported in this paper.

## CRediT authorship contribution statement

Y.N. Zan: Methodology, Investigation, Visualization, Writing - original draft. Q. Zhang: Investigation, Visualization, Writing - original draft. Y.T. Zhou: Investigation. Z.Y. Liu: Formal analysis. Q.Z. Wang: Project administration, Funding acquisition. D. Wang: Resources. B.L. Xiao: Conceptualization, Writing - review & editing, Funding acquisition. W.C. Ren: Resources, Data curation. Z.Y. Ma: Supervision, Writing - review & editing, Funding acquisition.

## Acknowledgments

The authors gratefully acknowledge the support of (a) Key Research Program of Frontier Sciences, CAS (No. QYZDJ-SSW-JSC015), (b) the National Key R & D Program of China (No. 2017YFB0703104), and (c) Youth Innovation Promotion Association CAS under grant No. 2016179.

## Appendix A. Supplementary data

Supplementary data to this article can be found online at <https://doi.org/10.1016/j.compositesb.2020.108095>.

## References

- [1] Gao YH, Yang C, Zhang JY, Cao LF, Liu G, Sun J, et al. Stabilizing nanoprecipitates in Al-Cu alloys for creep resistance at 300 °C. *Mater Res Lett* 2019;7(1):18–25.
- [2] Hu K, Xu Q, Ma X, Sun Q, Gao T, Liu X. A novel heat-resistant Al-Si-Cu-Ni-Mg base material synergistically strengthened by Ni-rich intermetallics and nano-AlNp microskeletons. *J Mater Sci Technol* 2019;35(3):306–12.
- [3] Li GJ, Liao HC, Suo XJ, Tang YY, Dixit US, Petrov P. Cr-induced morphology change of primary Mn-rich phase in Al-Si-Cu-Mn heat resistant aluminum alloys and its contribution to high temperature strength. *Mater Sci Eng A* 2018;709:90–6.
- [4] Poletti C, Balog M, Simancik F, Degischer HP. High-temperature strength of compacted sub-micrometer aluminium powder. *Acta Mater* 2010;58(10):3781–9.
- [5] Morri A, Ceschini L, Messieri S, Cerri E, Toschi S. Mo addition to the A354 (Al-Si-Cu-Mg) casting alloy: effects on microstructure and mechanical properties at room and high temperature. *Metals* 2018;8(6):18.
- [6] Skinner DJ, Bye RL, Raybould D, Brown AM. Dispersion strengthened Al-Fe-V-Si alloys. *Scripta Metall* 1986;20(6):867–72.
- [7] Franck RE, Hawk JA. Effect of very high-temperatures on the mechanical-properties of Al-Fe-V-Si alloy. *Scripta Metall* 1989;23(1):113–8.
- [8] Mitra S. Elevated-temperature mechanical-properties of a rapidly solidified Al-Fe-V-Si alloy. *Scripta Metall Mater* 1992;27(5):521–6.
- [9] W Chen YC, Fine Jr ME. Microstructural evolution and mechanical-properties of rapidly solidified Al-Zr-V alloys at high-temperatures. *Acta Metall Mater* 1990;38(5):771–80.
- [10] Lee JC, Lee S, Lee DY, Kim NJ. On the embrittlement of a rapidly solidified Al-Fe-V-Si alloy after high-temperature exposure. *Metall Trans A* 1991;22(4):853–8.
- [11] Khatri SC, Lawley A, Koczak MJ, Grassett KG. Creep and microstructural stability of dispersion-strengthened Al-Fe-V-Si-Er alloy. *Mater Sci Eng A* 1993;167(1–2):11–21.
- [12] Balog M, Krizik P, Nosko M, Hajovska Z, Riglos MVC, Rajner W, et al. Forged HITEMAL: Al-based MMCs strengthened with nanometric thick  $\text{Al}_2\text{O}_3$  skeleton. *Mater Sci Eng A* 2014;613:82–90.
- [13] Balog M, Hu T, Krizik P, Castro Riglos MV, Saller BD, Yang H, et al. On the thermal stability of ultrafine-grained Al stabilized by in-situ amorphous  $\text{Al}_2\text{O}_3$  network. *Mater Sci Eng* 2015;648:61–71.
- [14] Rufino B, Coulet MV, Bouchet R, Isnard O, Denoyel R. Structural changes and thermal properties of aluminium micro- and nano-powders. *Acta Mater* 2010;58(12):4224–32.
- [15] Rufino B, Poletti C, Simancik F, Walcher M, Rajner W. The effect of native  $\text{Al}_2\text{O}_3$  skin disruption on properties of fine Al powder compacts. *J Alloys Compd* 2011;509:S235–8.
- [16] Rufino B, Boulic'h F, Coulet MV, Lacroix G, Denoyel R. Influence of particles size on thermal properties of aluminium powder. *Acta Mater* 2007;55(8):2815–27.
- [17] Jeurgens LPH, Sloof WG, Tichelaar FD, Mittemeijer EJ. Thermodynamic stability of amorphous oxide films on metals: application to aluminum oxide films on aluminum substrates. *Phys Rev B* 2000;62(7):4707–19.
- [18] Reichel F, Jeurgens LPH, Richter G, Mittemeijer J. Amorphous versus crystalline state for ultrathin  $\text{Al}_2\text{O}_3$  overgrowths on Al substrates. *J Appl Phys* 2008;103(9).
- [19] Jeurgens LPH, Sloof WG, Tichelaar FD, Mittemeijer EJ. Structure and morphology of aluminium-oxide films formed by thermal oxidation of aluminium. *Thin Solid Films* 2002;418(2):89–101.

- [20] Yang ZQ, He LL, Chen J, Cong HT, Ye HQ. Microstructure and thermal stability of an ultrafine Al/Al<sub>2</sub>O<sub>3</sub> composite. *J Mater Res* 2003;18(2):272–8.
- [21] van Beek HJ, Mittemeijer EJ. Amorphous and crystalline oxides on aluminium. *Thin Solid Films* 1984;122(2):131–51.
- [22] Tabandeh-Khorshid M, Kumar A, Omrani E, Kim C, Rohatgi P. Synthesis, characterization, and properties of graphene reinforced metal-matrix nanocomposites. *Compos Part B* 2020;183:26.
- [23] Hedayatian M, Momeni A, Nezamabadi A, Vahedi K. Effect of graphene oxide nanoplates on the microstructure, quasi-static and dynamic penetration behavior of Al6061 nanocomposites. *Compos Part B* 2020;182:14.
- [24] Xie YM, Meng XC, Huang YX, Li JC, Cao J. Deformation-driven metallurgy of graphene nanoplatelets reinforced aluminum composite for the balance between strength and ductility. *Compos Part B* 2019;177:10.
- [25] Hwang J, Yoon T, Jin SH, Lee J, Kim T-S, Hong SH, et al. Enhanced mechanical properties of graphene/copper nanocomposites using a molecular-level mixing process. *Adv Mater* 2013;25(46):6724–9.
- [26] Yoo SC, Lee J, Hong SH. Synergistic outstanding strengthening behavior of graphene/copper nanocomposites. *Compos Part B* 2019;176:107235.
- [27] Ferreira F, Ferreira I, Camacho E, Lopes F, Marques AC, Velhinho A. Graphene oxide-reinforced aluminium-matrix nanostructured composites fabricated by accumulative roll bonding. *Compos Part B* 2019;164:265–71.
- [28] Jiang YY, Xu R, Tan ZQ, Ji G, Fan GL, Li Z, et al. Interface-induced strain hardening of graphene nanosheet/aluminum composites. *Carbon* 2019;146:17–27.
- [29] Shin SE, Ko YJ, Bae DH. Mechanical and thermal properties of nanocarbon-reinforced aluminum matrix composites at elevated temperatures. *Compos Part B* 2016;106:66–73.
- [30] Zan YN, Zhou YT, Liu ZY, Ma GN, Wang D, Wang QZ, et al. Enhancing strength and ductility synergy through heterogeneous structure design in nanoscale Al<sub>2</sub>O<sub>3</sub> particulate reinforced Al composites. *Mater Des* 2019;166:107629.
- [31] Wu G, Yu Z, Jiang L, Zhou C, Deng G, Deng X, et al. A novel method for preparing graphene nanosheets/Al composites by accumulative extrusion-bonding process. *Carbon* 2019;152:932–45.
- [32] Dasari BL, Morshed M, Nouri JM, Brabazon D, Naher S. Mechanical properties of graphene oxide reinforced aluminium matrix composites. *Compos Part B* 2018;145:136–44.
- [33] Li Z, Guo Q, Li ZQ, Fan GL, Xiong DB, Su YS, et al. Enhanced mechanical properties of graphene (reduced graphene oxide)/aluminum composites with a bioinspired nanolaminated structure. *Nano Lett* 2015;15(12):8077–83.
- [34] Şenel MC, Gürbüz M, Koç E. Fabrication and characterization of synergistic Al-SiC-GNPs hybrid composites. *Compos Part B* 2018;154:1–9.
- [35] Zhang Y, Li X. Bioinspired, graphene/Al<sub>2</sub>O<sub>3</sub> doubly reinforced aluminum composites with high strength and toughness. *Nano Lett* 2017;17(11):6907–15.
- [36] Huang Y, Bazarnik P, Wan DQ, Luo D, Pereira PHR, Lewandowska M, et al. The fabrication of graphene-reinforced Al-based nanocomposites using high-pressure torsion. *Acta Mater* 2019;164:499–511.
- [37] Zhou WW, Chen C, Mikulova P, Dong MQ, Fan YC, Kikuchi K, et al. Thermal expansion behaviors of few-layered graphene-reinforced Al matrix composites. *J Alloys Compd* 2019;792:988–93.
- [38] Zhang Q, Qian X, Thebo KH, Cheng H-M, Ren W. Controlling reduction degree of graphene oxide membranes for improved water permeance. *Sci Bull* 2018;63(12):788–94.
- [39] Li Z, Fan G, Tan Z, Guo Q, Xiong D, Su Y, et al. Uniform dispersion of graphene oxide in aluminum powder by direct electrostatic adsorption for fabrication of graphene/aluminum composites. *Nanotechnology* 2014;25(32):325601.
- [40] Nardone VC, Prewo KM. On the strength of discontinuous silicon carbide reinforced aluminum composites. *Scripta Metall* 1986;20(1):43–8.
- [41] Paredes JI, Villar-Rodil S, Solis-Fernandez P, Martinez-Alonso A, Tascon JMD. Atomic force and scanning tunneling microscopy imaging of graphene nanosheets derived from graphite oxide. *Langmuir* 2009;25(10):5957–68.
- [42] Gahlot S, Sharma PP, Gupta H, Kulshrestha V, Jha PK. Preparation of graphene oxide nano-composite ion-exchange membranes for desalination application. *RSC Adv* 2014;4(47):24662–70.
- [43] Xu W, Wu X, Honma T, Ringer SP, Xia K. Nanostructured Al–Al<sub>2</sub>O<sub>3</sub> composite formed in situ during consolidation of ultrafine Al particles by back pressure equal channel angular pressing. *Acta Mater* 2009;57(14):4321–30.
- [44] Liu J, Khan U, Coleman J, Fernandez B, Rodriguez P, Naher S, et al. Graphene oxide and graphene nanosheet reinforced aluminium matrix composites: powder synthesis and prepared composite characteristics. *Mater Des* 2016;94:87–94.
- [45] Yu ZH, Yang WS, Zhou C, Zhang NB, Chao ZL, Liu H, et al. Effect of ball milling time on graphene nanosheets reinforced Al6063 composite fabricated by pressure infiltration method. *Carbon* 2019;141:25–39.
- [46] Zhou W, Dong M, Zhou Z, Sun X, Kikuchi K, Nomura N, et al. In situ formation of uniformly dispersed Al<sub>4</sub>C<sub>3</sub> nanorods during additive manufacturing of graphene oxide/Al mixed powders. *Carbon* 2019;141:67–75.
- [47] Zhou W, Mikulova P, Fan Y, Kikuchi K, Nomura N, Kawasaki A. Interfacial reaction induced efficient load transfer in few-layer graphene reinforced Al matrix composites for high-performance conductor. *Compos Part B* 2019;167:93–9.
- [48] Zhou YT, Zan YN, Zheng SJ, Wang QZ, Xiao BL, Ma XL, et al. Distribution of the microalloying element Cu in B4C-reinforced 6061Al composites. *J Alloys Compd* 2017;728(Supplement C):112–7.
- [49] Zan YN, Zhou YT, Zhao H, Liu ZY, Wang QZ, Wang D, et al. Enhancing high-temperature strength of (B4C+Al<sub>2</sub>O<sub>3</sub>)/Al designed for neutron absorbing materials by constructing lamellar structure. *Compos Part B* 2020;183:107674.
- [50] Shen YF, Guan RG, Zhao ZY, Misra RDK. Ultrafine-grained Al–0.2Sc–0.1Zr alloy: the mechanistic contribution of nano-sized precipitates on grain refinement during the novel process of accumulative continuous extrusion. *Acta Mater* 2015;100:247–55.
- [51] Nikulin I, Kipelova A, Malopheyev S, Kaibyshev R. Effect of second phase particles on grain refinement during equal-channel angular pressing of an Al–Mg–Mn alloy. *Acta Mater* 2012;60(2):487–97.
- [52] Barlow CY, Hansen N, Liu YL. Fine scale structures from deformation of aluminium containing small alumina particles. *Acta Mater* 2002;50(1):171–82.
- [53] Prados EF, Sordi VL, Ferrante M. The effect of Al<sub>2</sub>Cu precipitates on the microstructural evolution, tensile strength, ductility and work-hardening behaviour of a Al–4wt.% Cu alloy processed by equal-channel angular pressing. *Acta Mater* 2013;61(1):115–25.
- [54] Lee H, Lee N, Seo Y, Eom J, Lee S. Comparison of frictional forces on graphene and graphite. *Nanotechnology* 2009;20(32):325701.
- [55] Filleter T, McChesney JL, Bostwick A, Rotenberg E, Emtsev KV, Seyller T, et al. Friction and dissipation in epitaxial graphene films. *Phys Rev Lett* 2009;102(8):086102.
- [56] Lin L-Y, Kim D-E, Kim W-K, Jun S-C. Friction and wear characteristics of multi-layer graphene films investigated by atomic force microscopy. *Surf Coating Technol* 2011;205(20):4864–9.
- [57] Lee C, Wei X, Li Q, Carpick R, Kysar JW, Hone J. Elastic and frictional properties of graphene. *Phys Status Solidi* 2009;246(11–12):2562–7.
- [58] Lee C, Li Q, Kalb W, Liu X-Z, Berger H, Carpick RW, et al. Frictional characteristics of atomically thin sheets. *Science* 2010;328(5974):76–80.
- [59] Zan YN, Zhang Q, Zhou YT, Wang QZ, Xiao BL, Ma ZY. Enhancing high-temperature strength of B4C–6061Al neutron absorber material by in-situ Mg(Al) B<sub>2</sub>. *J Nucl Mater* 2019;526:151788.
- [60] Zan YN, Zhou YT, Liu ZY, Wang QZ, Wang WG, Wang D, et al. Microstructure and mechanical properties of (B4C+Al<sub>2</sub>O<sub>3</sub>)/Al composites designed for neutron absorbing materials with both structural and functional usages. *Mater Sci Eng* 2020;773:138840.